JOC The Journal of Organic Chemistry

Article

Toward a Predictive Understandings of Phosphine-Catalyzed [3+2] Annulation of Allenoates with Acrylate or Imine

Zhaoyuan Yu, Zhichao Jin, Meng Duan, Ruopeng Bai, Yixin Lu, and Yu Lan

J. Org. Chem., **Just Accepted Manuscript** • DOI: 10.1021/acs.joc.8b01259 • Publication Date (Web): 16 Aug 2018

ACS Publications

is published by the American Chemical Society. 1155 Sixteenth Street N.W., Washington, DC 20036

induction. The theoretical calculation results agreed with experimental observations, and these results provide valuable insight into catalyst design and understanding of mechanisms of related reactions.

INTRODUCTION

Organophosphorus compounds have received considerable attention in the past few decades.[1] Phosphines are typically used as ligands[2] in transition metal-mediated processes,[3] but they are also widely used as nucleophilic catalysts in organic synthesis owing to their nucleophilicity.[4] The past decade has seen remarkable progress of phosphine-catalyzed organic reactions, e.g. the Rauhut–Currier reaction,[5] Morita–Baylis–Hillman reaction,[6] and Michael addition,[7] among others.[8] In 1995, Lu and co-workers disclosed a phosphine-catalyzed [3+2] cycloaddition of allenoates to activated alkenes, which has become one of the most well-established methods for the construction of five-membered ring systems (Scheme 1, eq. a).[9] Over the time, various chiral phosphine catalysts have been developed for asymmetric [3+2] annulation reactions. Zhang et al. developed a chiral phosphine with a unique fused bicyclic [2.2.1] ring, which was shown to catalyze the [3+2] cyclization between 2,3-butadienoates and activated alkenes with excellent regio- and enantioselectivity (eq. b).[10] The Fu group reported a highly enantioselective [3+2] cycloaddition of allenoates to enones catalyzed by a C_2-symmetric chiral phosphine catalyst (eq. c).[11] Miller and co-workers designed a multifunctional phosphine-containing α-amino acid, which was utilized to catalyze an enantioselective [3+2] cycloaddition of allenoate to tetralone (eq. d).[12] Undoubtedly, phosphine-catalyzed asymmetric [3+2] annulations of allenes with activated alkenes have been well recognized as one of the most efficient synthetic methods for the construction of enantiomerically enriched five-membered cyclic structural motifs.[13]

Scheme 1. Selected Examples of Phosphine Catalyzed [3+2] Cycloaddition Reactions

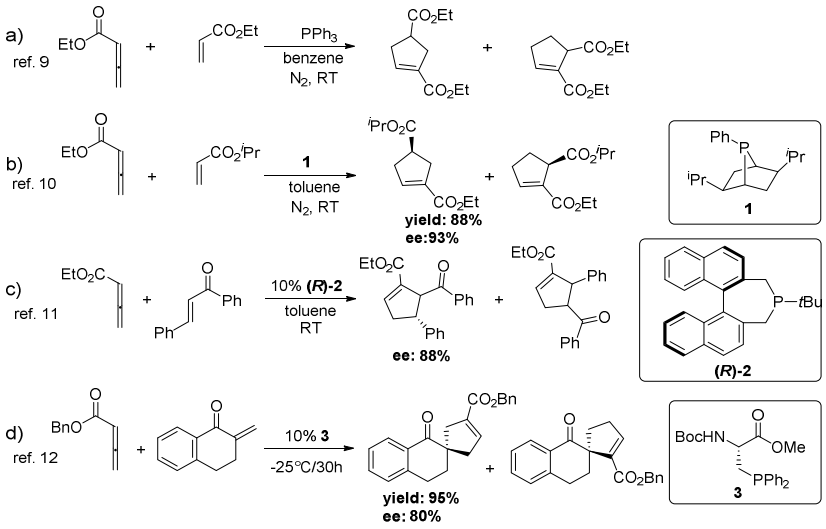

For the creation of new stereogenic centers in a catalytic reaction, the asymmetric induction is determined by the chiral catalysts utilized, the chiral environments of which are of vital importance.[14] Amino acids are arguably the most abundant, inexpensive, and readily available chiral building blocks in nature,[15] thus they are widely used in asymmetric synthesis.[16] In 2011, we introduced a new family of dipeptide-based phosphine catalysts, and showed their effectiveness in promoting asymmetric [3+2] annulation reactions.[17] As illustrated in Scheme 2, D-Thr-L-*tert*-Leu-based phosphine **P1** catalyzed allenoate–acrylate [3+2] cyclization and afforded the desired adduct in 95% yield and 74% *ee*. Subsequently, we demonstrated application of this powerful catalyst in asymmetric [3+2] annulation between imines and allenoates.[18] Although the mechanisms of phosphine-catalyzed [3+2] annulations have been investigated by experimentally and computationally in previous studies,[19] elucidation of stereoselectivities of phosphine-promoted catalytic processes is still very limited. In our initial disclosures, we proposed that our bifunctional phosphine catalysts interact with substrates, e.g. acrylate or imine, through hydrogen bonding interactions, which were believed to be the key to the observed stereoselectivity. Herein, we carry out

computational studies to elucidate the reaction mechanism, and present the origin of enantioselectivity observed in the phosphine-catalyzed [3+2] annulation between allenoates and acrylate or imine.

Scheme 2. Dipeptide-functionalized Phosphine Catalyzed [3+2] Cycloaddition between Allenoates and Acrylate or Imine.

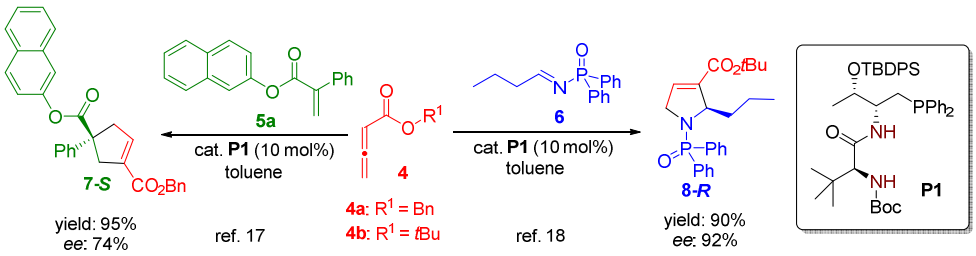

COMPUTATIONAL METHODS

All the DFT calculations were carried out with the GAUSSIAN 09 series of programs.[20] Density functional B3LYP[21] with a standard 6-31G(d) basis set[22] was used for geometry optimizations. Harmonic vibrational frequency calculations were performed with the same method for all stationary points to confirm them as a local minima or transition structures and to derive the thermochemical corrections for the enthalpies and free energies. Recent works from our group[23] showed that M11 functional,[24] recently proposed by the Truhlar group could give more accurate energetic information. Here we used the M11 functional with the larger basis set 6-311+G(d)[25] to derive single-point energies on B3LYP/6-31G(d) optimized geometries. The solvent effects were considered by single point calculations using IEFPCM model (toluene).[26] The thermal corrections evaluated from the vibrational frequencies at B3LYP/6-31G(d) level on the optimized geometries were then added to the M11/6-311+G(d) electronic energies to obtain the free energies. The NCIPLOT analyses were

conducted with Multiwfn[27] and VMD.[28] The 3D images of the calculated structures were prepared using CYLview.[29]

RESULTS AND DISCUSSION

Mechanism for Phosphine-Catalyzed [3+2] Cycloaddition. On the basis of Lu's pioneering work[9] and relevant computational studies,[30] the commonly accepted mechanism of phosphine-catalyzed [3+2] cycloaddition is shown in Scheme 3. Phosphine catalyst **P1** adds on to allenoate **4** to yield the zwitterionic intermediate **A**. In the left cycle (allenoate–acrylate cyclization), the [3+2] the cycloaddition process between intermediate **A** and acrylate **5a** is stepwise and affords intermediate **C**. The following proton transfer gives intermediate **D**, which then eliminates catalyst **P1** and forms the annulation product **7**. For the allenoate–imine cyclization, the addition of the zwitterionic intermediate **A** to imine **6** generates intermediate **E**, which undergoes intramolecular cyclization followed by proton transfer to furnish intermediate **G**. Subsequent elimination of the phosphine then affords annulation product **8**. In the above proposal, the first C–C bond-forming step was deemed to be the enantiodetermining step in both cycles, and the non-covalent interactions between catalysts and substrates are believed to be crucial in stabilizing the key transition states, leading to the formation of major stereoisomer.

Scheme 3. Mechanism for [3+2] Cycloaddition Catalyzed by Dipeptide-Functionalized Phosphine P1

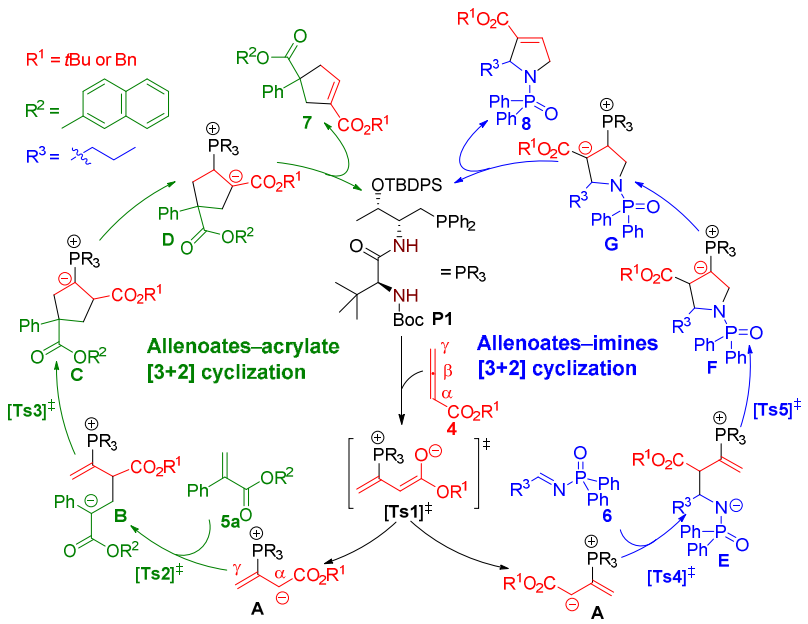

Jacobsen,[31] Jørgensen,[32] Goodman,[33] Houk[34] and others[35] have shown that non-covalent interactions between catalysts and substrates have marked effects in controlling the enantioselectivities through a combination of experimental and theoretical investigations.[36] Cowen and Miller proposed the intramolecular hydrogen bond induced the selectivity in phosphine-catalyzed [3+2] cycloaddition of allenoates and enones.[12] The intermolecular hydrogen bond model was also proposed by Fang and Jacobsen for the [3+2] annulation of an imine with allenoate.[37] Our experimental and theoretical results also validated the importance of hydrogen-bonding interactions between substrates and catalysts in the phosphine-catalyzed γ-additions of oxazolones to 2,3-butadienoates.[38]

In our dipeptide-based bifunctional phosphine **P1**, there are two possible hydrogen donors (two N–H moieties), however, their exact roles in controlling the stereoselectivities of the reaction remain to be clarified. In the previous investigation (Table 1), catalyst **P2** was identified as a slightly superior catalyst to **P1** (78% *ee* versus 74% *ee*) (entries 1 & 2). Among the different acrylate esters, alkyl substituted acrylate (*i*-Pr) was found to be an inferior substrate (entry 3), in contrast, aryl-substituted

acrylates were excellent substrates, furnishing the desired adducts in good yields and high *ee* values (entries 4, 5 and 6). Strikingly, acrylate bearing a 9-phenanthryl group led to excellent enantioselectivity (91 % *ee*), this was in comparison to the acrylates bearing a 2-naphthyl group (84 % *ee*) or phenyl group (76 % *ee*). The employment of acrylates with different aryl substituents resulted in the formation of [3+2] annulation products with much differentiated enantioselectivities, which simply suggested that those substituents may play an important role in asymmetric induction.

Table 1. Optimization of Reaction Condition[a]

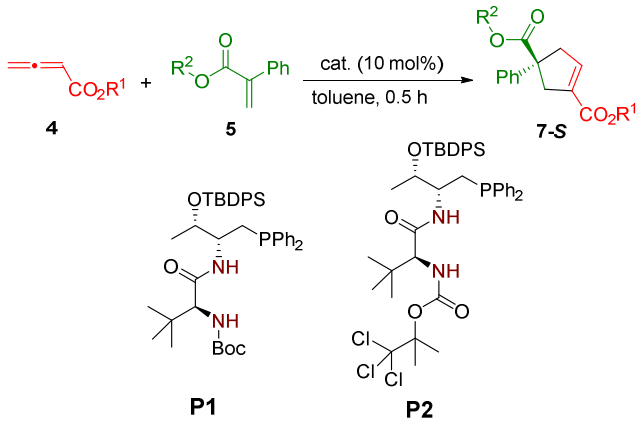

Entry	Catalyst	R^1	R^2	α:γ[b]	Yield [%][c]	*ee* [%][d]
1	**P1**	Bn	2-naphthyl	94:6	95	74
2	**P2**	Bn	2-naphthyl	95:5	96	78
3	**P2**	*t*-Bu	*i*-pr	97:3	72	24
4	**P2**	*t*-Bu	Ph	97:3	92	76
5	**P2**	*t*-Bu	2-naphthyl	96:4	94	84
6	**P2**	*t*-Bu	9-phenanthryl	>99:1	95	91

[a] Reactions were performed with **5** (0.05 mmol), **4** (0.075 mmol) and Phosphine catalysts (10 mol %) in toluene (1.0 mL) at room temperature. [b] Determined by ^{1}H NMR analysis of the crude reaction mixture. [c] Isolated yield. [d] The *ee* value of the major stereoisomer, determined by HPLC analysis on a chiral stationary phase.

To further probe the reaction mechanistically, we designed a number of analogous L-Val-containing dipeptide phosphine catalysts and examined their catalytic effects in the [3+2] annulation between allenoates and acrylates (Table 2). Synthetically, catalysts **P3** to **P5** were more readily accessible, and the catalytic effects of **P3** is comparable to that of catalyst **P1**. When the hydrogen at the terminal amino group of the L-Val residue was substituted by a methyl group (catalyst **P4**), the observed *ee* value was 60%, not substantially lower than that attainable by using catalyst **P3**. However, substitution of the amide N–H with a methyl group (catalyst **P5**), led to much decreased ee value of 18%, and the configuration of the product was also reversed. The above results suggested that the amide N–H group is of pivotal importance in asymmetric induction, and the presence of the carbamate N–H seems to be less important.

Table 2. Different phosphine catalyzed [3+2] cycloaddition reaction[a]

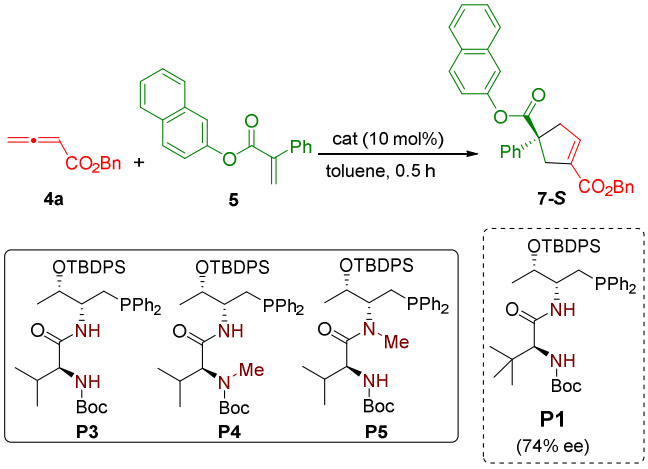

Entry	catalyst	Yield [%][b]	*ee* [%][c]
1	**P3**	>99%	73
2	**P4**	>99%	60
3	**P5**	59%	-18

[a] Reactions were performed with **5** (0.05 mmol), **4a** (0.075 mmol) and phosphine catalysts (10 mol %) in toluene (1.0 mL) at room temperature. [b] Isolated yield. [c] The *ee* value of the major stereoisomer, determined by HPLC analysis on a chiral stationary phase.

Scheme 4. Proposed Structures of Transition States in Enantioselectivity Determining Step

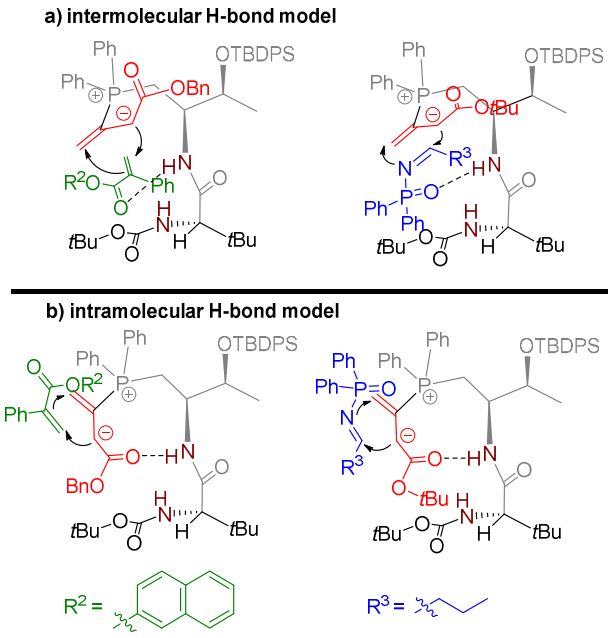

Based on the above experimental results, we proposed two possible models and further explored the [3+2] annulations computationally (Scheme 4). In the intermolecular H-bond model (Scheme 4a), the interactions between amide moiety of the catalyst with acrylate or imine contribute significantly to the key transition state leading to the formation of the major stereoisomer. Both acrylate and imine are arranged in the bulky pocket of the catalyst, and there are significant steric repulsion between catalyst and substrates. Alternatively, we propose that the carbonyl group of allenoate interacts with amide through intramolecular H-bond, thus ensuring selectivity in the subsequent nucleophilic attack (Scheme 4b). When acrylates are used as a substrate, the non-covalent interactions between the 2-naphthyl group of the acrylate and the phenyl group of phosphine catalyst stabilize the cycloaddition transition states. Similarly, when imines are used as a reaction partner, the non-covalent interactions between phenyl group of imine and catalyst possible exists only in the energetically favored transition state leading to the major enantiomer.

Activation Barrier of Phosphine Addition to Allenoate. A complete energy profile of a model reaction based on the phosphine catalyst **P1** was described. As shown in Figure 1, the

hydrogen-bonding complex **9-A** is formed from the active catalyst **P1** and allenoate **4a** with a free energy increase of 3.7 kcal/mol, although the bonding energy of the formed hydrogen bond is about 7.2 kcal/mol as the reaction enthalpy. The nucleophilic addition of phosphine takes place via transition state **Ts1-A** with an overall barrier of 20.4 kcal/mol, leading to intermediate **10-A**. When substrate is replaced by allenoate **4b**, the calculations predict an overall barrier of 18.8 kcal/mol for nucleophilic addition step.

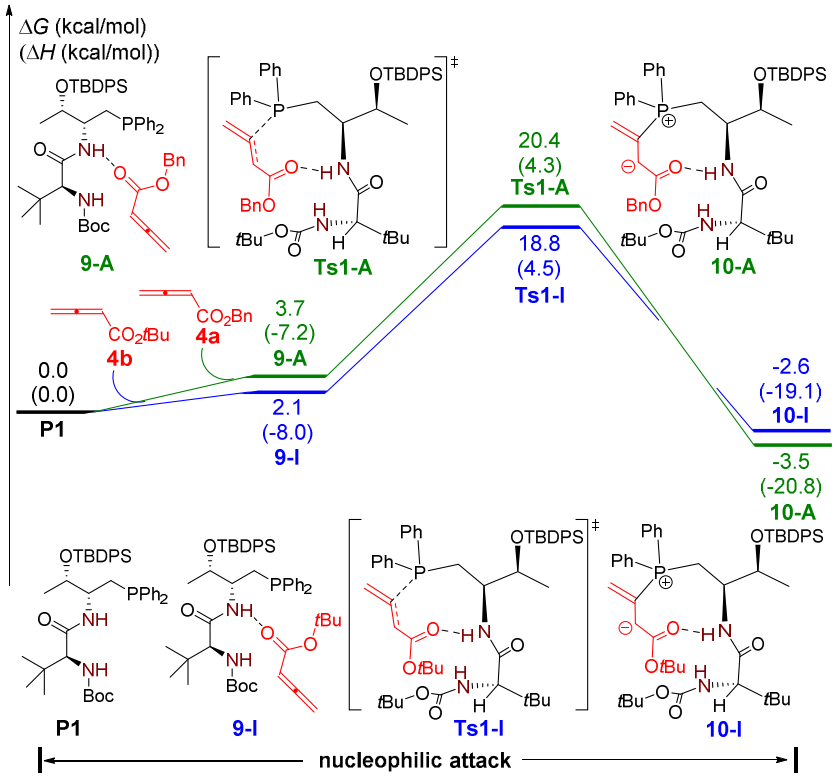

Figure 1. Energy profile for the nucleophilic attack step.

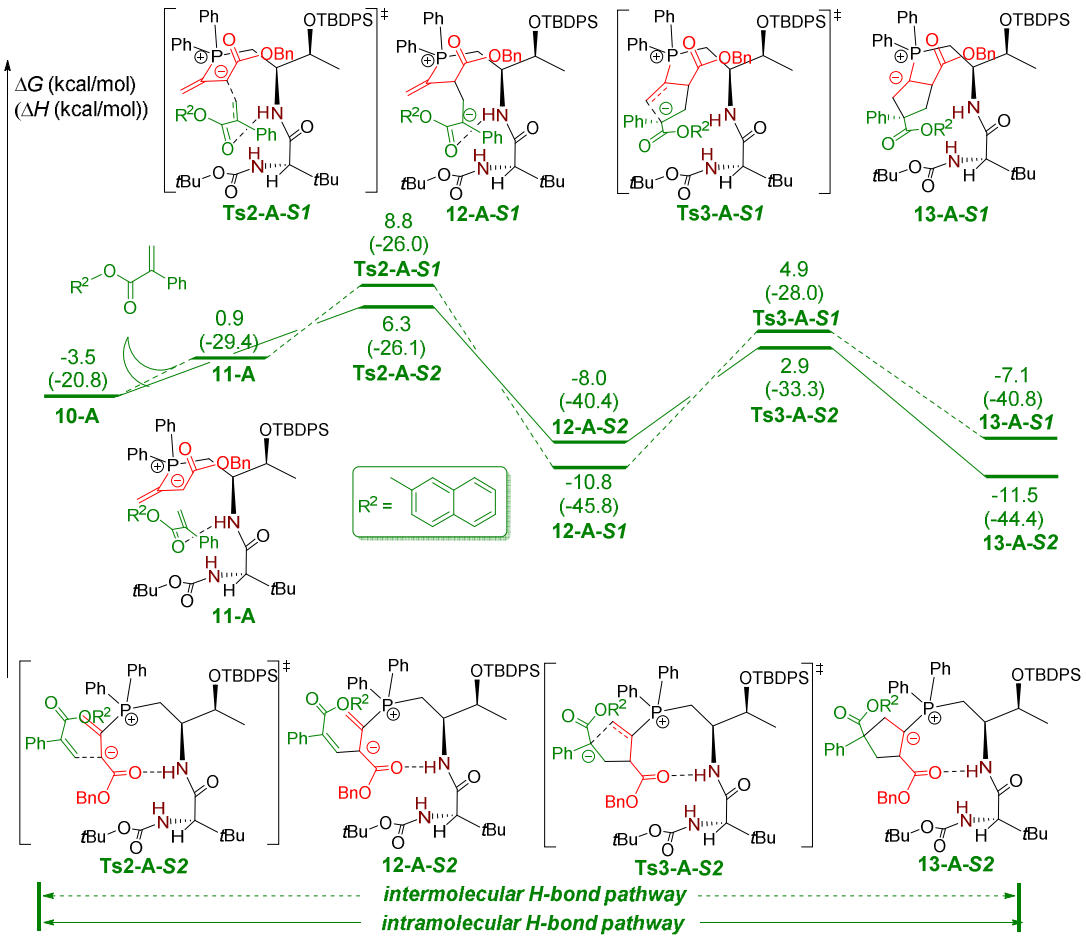

Figure 2. The DFT computed competing pathways of dipeptide-functionalized phosphine **P1** catalyzed [3+2] annulation of acrylate with allenoates.

Reaction with Acrylate. We initially chose 2-naphthyl-substituted acrylate to perform DFT computations to elucidate the reaction mechanism, as well as origins of observed enantioselectivities. As shown in Figure 2, from intermediate **10-A**, both intermolecular H-bond and intramolecular H-bond model were investigated in detail. In the intramolecular H-bond pathway, the amide group of catalyst interacts with allenoate by a single hydrogen bond, and the lowest energy transition state **Ts2-A-*S2*** was located for the nucleophilic attack step with a barrier of 9.8 kcal/mol. The subsequent ring closure occurs *via* transition state **Ts3-A-*S2*** to form the intermediate **13-A-*S2*** with a five-membered ring (the free energy surface for proton transfer from **13-A-*S2***, regenerate phosphine catalyst **P1** is given in Fig. S6 of Supporting Information.). **Ts3-A-*S2*** is 3.4 kcal/mol more stable

than **Ts2-A-*S2***. The intermolecular H-bond pathway was also considered. However, the transition state **Ts2-A-*S1*** is energetically less favorable compared to **Ts2-A-*S2*** by 2.5 kcal/mol. The computational studies illustrate that phosphine catalyst **P1** catalyzes allenoate–acrylate [3+2] annulation through intramolecular H-bond model more favorable than intermolecular H-bond, and the enantioselectivity is determined at the step where the zwitterionic species is added to the acrylate substrate.

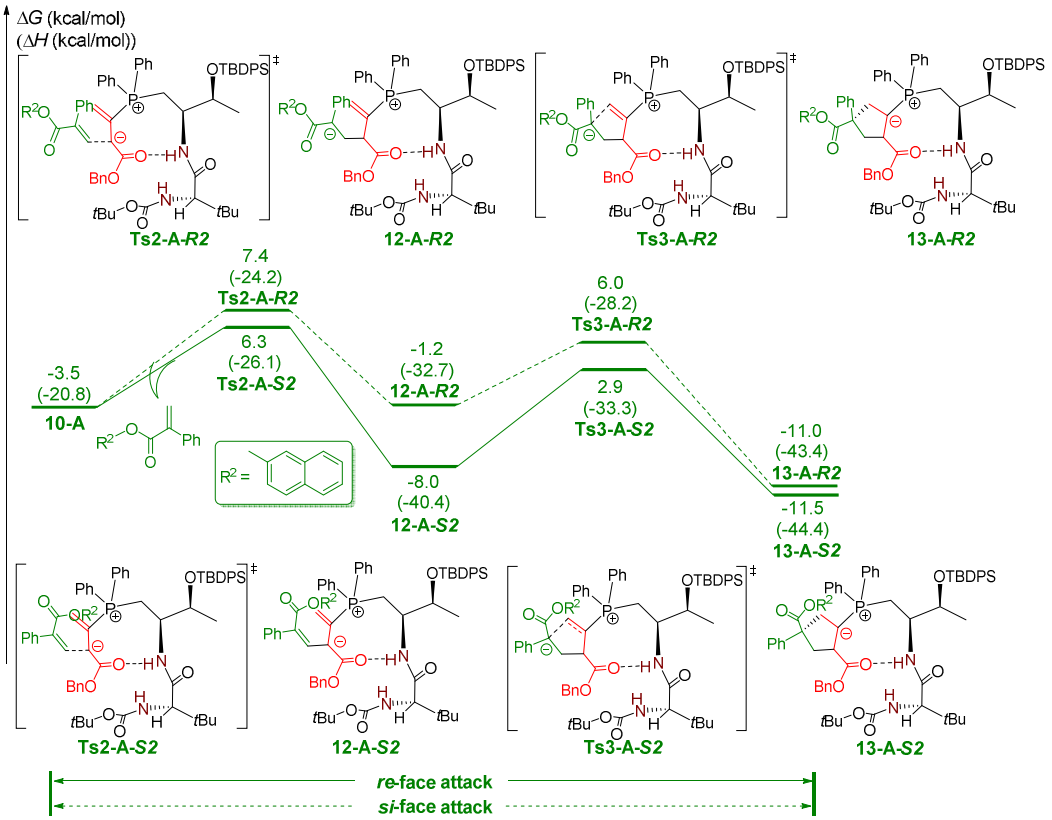

Figure 3. Free energy profiles for phosphine **P1** catalyzed [3+2] annulation of acrylate with allenoates leading to the enantiomer **7-*R*** (green dashed line) and **7-*S*** (green line).

In order to elucidate the origin of enantioselectivity, the alternative pathway (the *si*-face attack) was calculated. As shown in Figure 3, the reaction pathway *via* the transition states **Ts2-A-*R2*** and **Ts3-A-*R2*** leads to the formation of enantiomer **7-*R***. The relative free energy of the transition state

Ts2-A-*S2* is 1.1 kcal/mol lower than that of **Ts2-A-*R2***, which indicates that **7-*S*** is the major product. The energy difference between **Ts2-A-*R2*** (*si*-face) and **Ts2-A-*S2*** (*re*-face) corresponds to an *ee* value of 73%, which agrees well with the experimental observations.

On the basis of the above calculations, we compare the two competing transition states (**Ts2-A-*R2*** and **Ts2-A-*S2***) (Figure 4a). Both have an almost linear H-bond between amide group of catalyst and allenoate. However, the forming C–C bond length in **Ts2-A-*S2*** is 0.09Å longer than that in **Ts2-A-*R2***, therefore, the transition state **Ts2-A-*S2*** occurs earlier than **Ts2-A-*R2***. In the case of **Ts2-A-*R2***, the C–C bond length is 3.86 Å, suggested that the phenyl group of acrylate associations with TBDPS group of phosphine catalyst **P1** *via* weak non-covalent interaction. Inspection of **Ts2-A-*S2*** shows that carbonyl group of acrylate is orientated towards one of the phenyl ring of the catalyst (O…H distance 2.28 Å), and the distance between the bigger aromatic ring naphthalenyloxy with OTBDPS is 4.00 Å. Consequently, the stronger non-covalent interactions in **Ts2-A-*S2*** make the *re*-face pathway more favorable than *si*-face pathway (**Ts2-A-*R2***). To better describe the non-covalent interactions, a visualization analysis[39] is made to understand the nature of non-covalent interactions in **Ts2-A-*S2*** and **Ts2-A-*R2***. As shown in Figure 4b, the critical interactions are labelled with red circles. In **Ts2-A-*R2***, the phenyl group of acrylate is perpendicular to the phenyl group of TBDPS group and it brings about significant non-covalent interactions. Whereas in **Ts2-A-*S2***, 2-naphthyl group is perpendicular to the phenyl group of TBDPS group. Furthermore, in **Ts2-A-*S2***, the carbonyl group of acrylate orients towards one of phenyl ring on the phosphine atom, thereby increases non-covalent interactions. As a result, **Ts2-A-*S2*** is more stable than **Ts2-A-*R2***, leading to the formation of the major enantiomer **7-*S***.

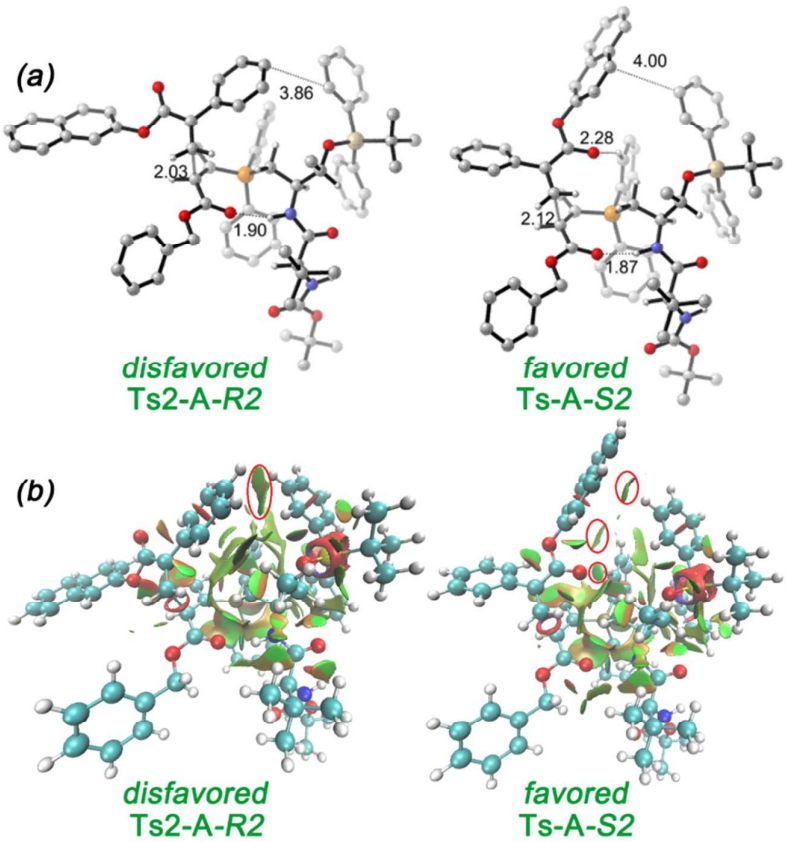

Figure 4. (a) Optimized structures of **Ts2-A-*R2*** and **Ts2-A-*S2***. Noncritical hydrogen atoms are omitted for clarity. Distances are given in angstroms and angles in degrees. (b) NCIPLOT of **Ts2-A-*R2*** and **Ts2-A-*S2*** transition states. The s = 0.6 au isosurface is colored according to a BGR scheme over the range $-0.05 < \mathrm{sign}(\lambda_2)\rho < 0.05$ au. Blue indicates strong attraction weak interaction, green indicates very weak interaction, and red indicates strong repulsion.

Reaction with Imine. The reaction mechanism is similar to that of the annulation between acrylates and alleonoates. Both intermolecular H-bond pathway and intramolecular H-bond pathway of phosphine catalyzed [3+2] annulation of imine with allenoates are summarized in Figure 5. In the intramolecular H-bond pathway, intermediate **10-I** undergoes C–C bond formation via transition state **Ts2-I-*R2*** to give the **12-I-*R2*** with a barrier of 14.1 kcal/mol. Subsequent C–N bond formation

(**Ts3-I-*R2***) requires an even higher activation energy than **Ts2-I-*R2*** and gives the stable intermediate **13-I-*R2***. On the other hand, the catalyst could activate the cyclization by forming an intermolecular hydrogen bond with imine substrate. From intermediate **11-I**, initial C–C bond formation via intermolecular H-bond transition state **Ts2-I-*R1*** has a barrier of 7.3 kcal/mol, leading to a more stable intermediate **12-I-*R1***, which then undergoes C–N bond formation *via* transition state **Ts3-I-*R1***, requiring a barrier of 14.5 kcal/mol (the free energy surface for proton transfer from **13-I-*R1***, regenerate phosphine catalyst **P1** is given in Fig. S7 of Supporting Information). Therefore, phosphine-catalyzed [3+2] annulation of imine with allenoate prefers the intermolecular H-bond model.

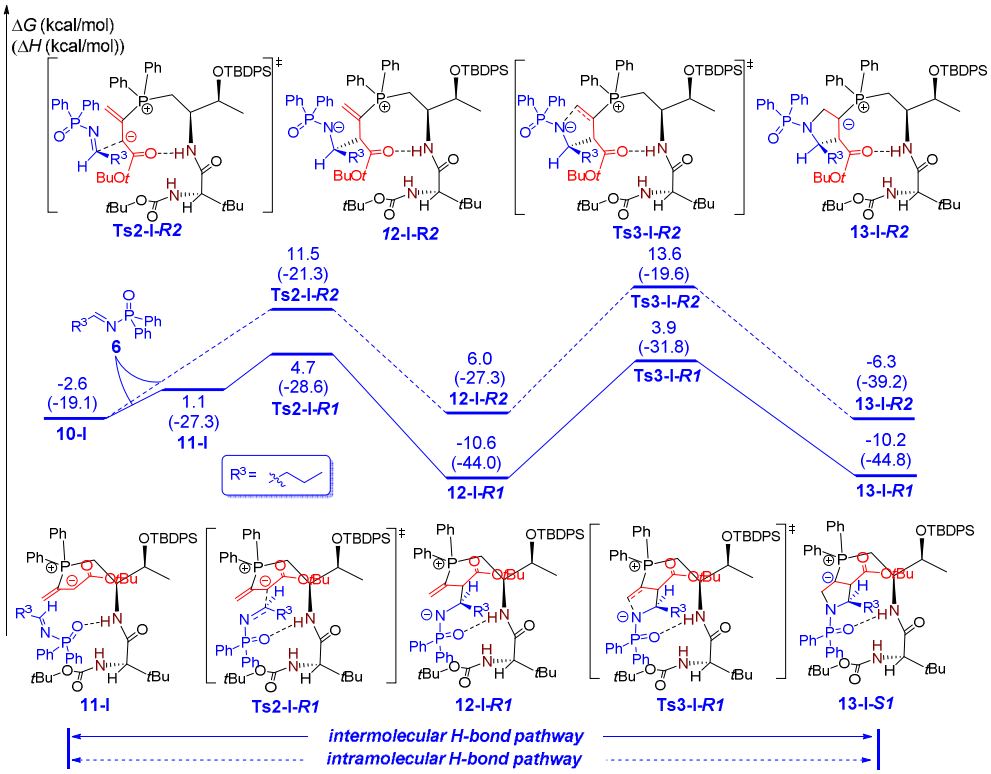

Figure 5. The DFT computed competing pathways of dipeptide-functionalized phosphine **P1** catalyzed [3+2] annulation of imine with allenoates.

To explore the origins of enantioselectivity, we then examined the free energy profile of the *re*-face attack pathway. As shown in Figure 6, the *re*-face attack pathway is predicted to be unfavorable than *si*-face attack pathway. The free energy of C–C bond forming transition state **Ts2-I-*S1*** is almost the same as that in **Ts2-I-*R1***. For *re*-face attack pathway, generate **12-I-*S1*** via **Ts2-I-*S1*** is an easy process. However, the subsequent ring closure take place via **Ts3-I-*S1*** is a hard process, causing **12-I-*S1*** prefer regenerate **11-I** via **Ts2-I-*S1***. Because of intermediate **12-I-*R1*** is more stable than **12-I-*S1***, leading to the position of equilibrium between **12-I-*S1*** and **12-I-*R1*** must favor **12-I-*R1***. Therefore, the formation *S*-configuration intermediate **13-I-*S1*** through transition state **Ts3-I-*S1*** with an energy barrier of 18.9 kcal/mol relate to **12-I-*R1***.

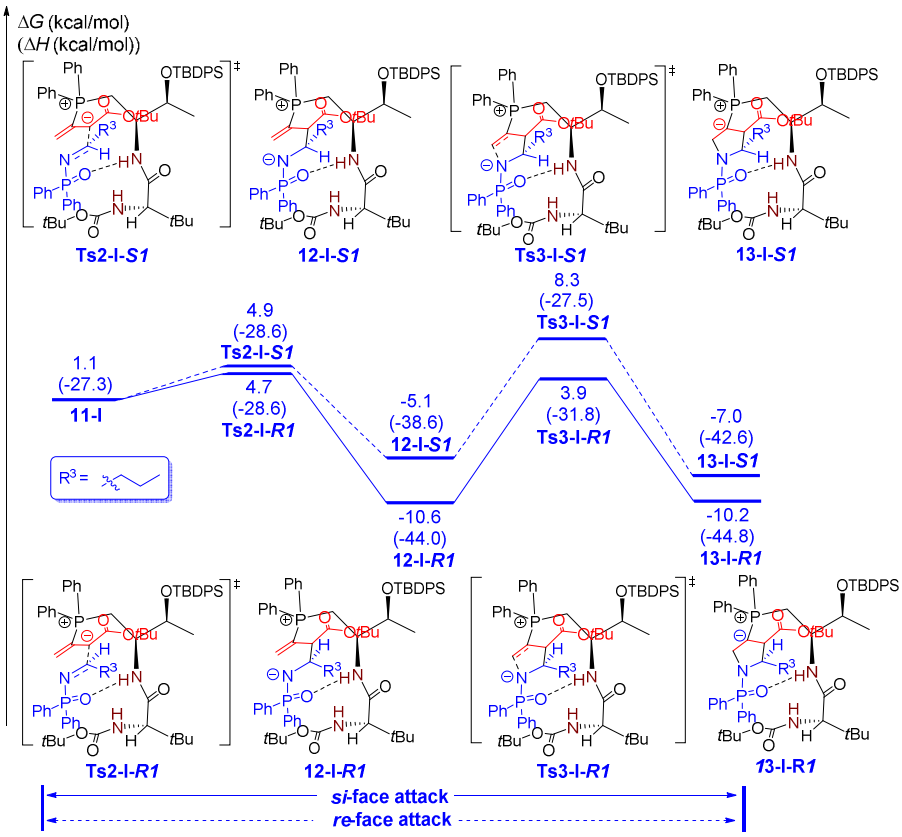

Figure 6. Free energy profiles for phosphine **P1** catalyzed [3+2] annulation of imine with allenoates leading to the enantiomer **8-*R*** (blue line) and **8-*S*** (blue dashed line).

The optimized structures of **Ts2-I-*R1*** and **Ts3-I-*S1*** are shown in Figure 7(a), structural analysis indicates that the steric interactions would be the major factors controlling the observed enantioselectivity. The hydrogen atom is oriented toward the pocket of catalyst in **Ts2-I-*R1***, the shortest H–H distance between imine and catalyst is 2.79 Å. In contrast, the sterically demanding *n*-propyl group is oriented toward the pocket of catalyst and responsible for the unfavorable steric interactions in **Ts3-I-*S1***. Thus, phosphine-catalyzed [3+2] annulation of imine with allenoate preferentially proceeds via the *si*-face attack pathway. As shown in Figure 7b, there are weak repulsions between imine and catalyst (red circles labelled) in **Ts3-I-*S1***.

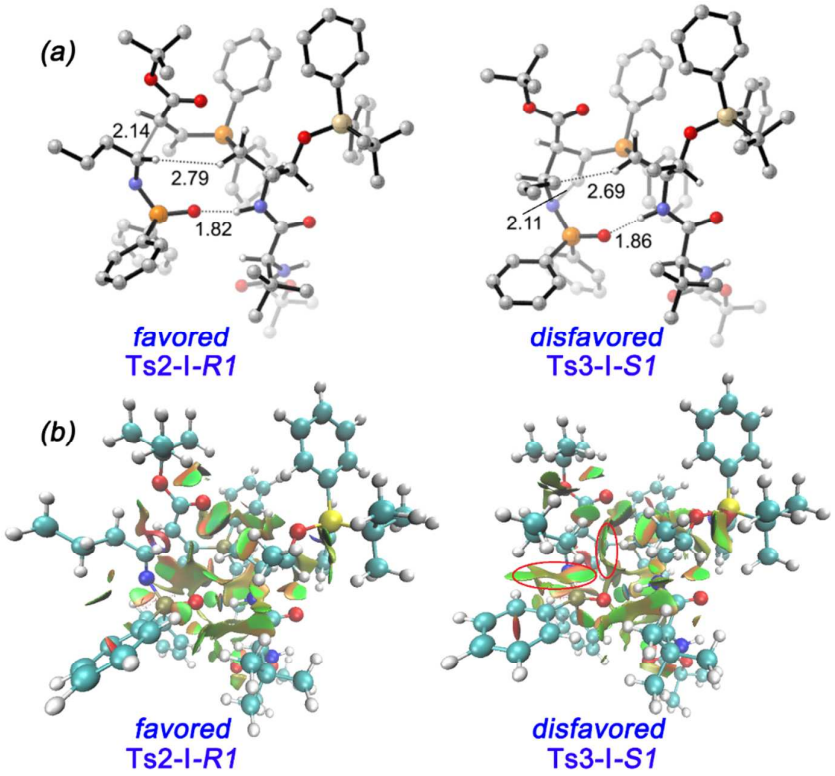

Figure 7. (a) Optimized structures of **Ts2-I-*R1*** and **Ts3-I-*S1***. Noncritical hydrogen atoms are omitted for clarity. Distances are given in angstroms and angles in degrees. (b) NCIPLOT of **Ts2-I-*R1*** and **Ts2-3-*S1*** transition states. The s = 0.6 au isosurface is colored according to a BGR

scheme over the range -0.05 < sign(λ_2)ρ < 0.05 au. Blue indicates strong attraction weak interaction, green indicates very weak interaction, and red indicates strong repulsion.

Catalyst Evaluation. Based on our calculation analysis, we look forward provide theoretical guidance and facilitate the design of more effective catalytic systems. As shown in Table 1 (entry 1 and 2), phosphine catalyst **P1** catalyzed [3+2] cycloaddition between allenoate **4a** and acrylate **5** afford the *S*-configuration product with 74% *ee* value. As mentioned above, the terminal NHBoc group seems to have less impact for enantioselectivity and this moiety should be replaceable. Therefore, we suspect that the catalyst **P6** could provide better result, due to the trifluoromethyl group substituted phenyl ring is coplanar with amide group and leading to an additional non-covalent interactions between allenoate and catalyst. The NCIPLOT of **10-A-P6** verified our hypothesis, apart from the H-bond between allenoate and catalyst, additional stabilizing non-covalent interactions between allenoate and substituted phenyl ring on the catalyst were identified (Figure 9b). More importantly, as shown in Figure 8, calculated free energy profile indicate that *re*-face attack pathway is much favor than *si*-face attack pathway and in consistent with experimental observed (>99 yield, 92% *ee*).

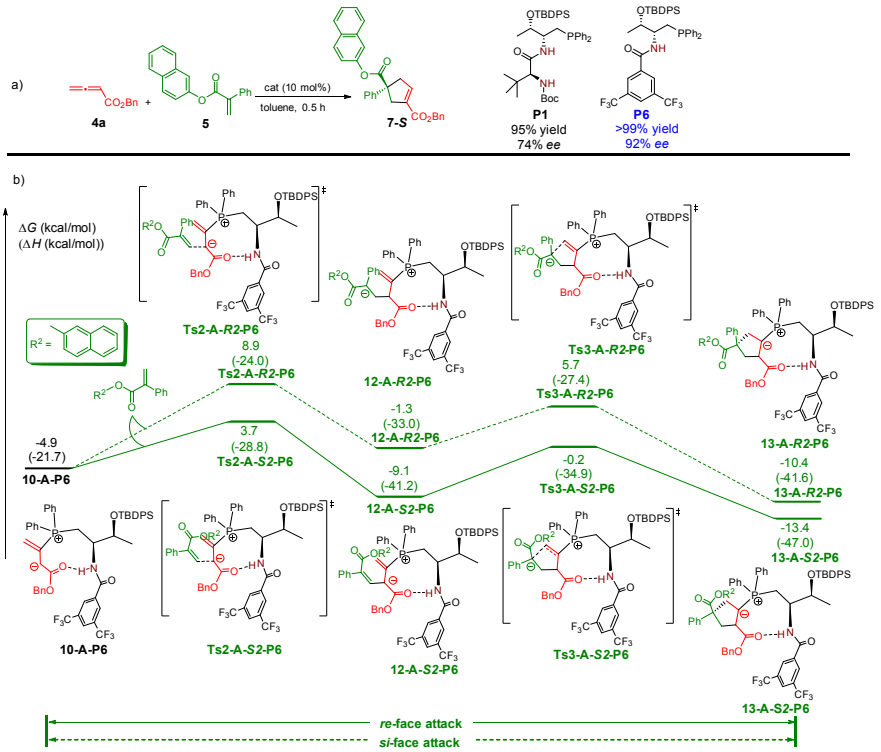

Figure 8. The DFT computed competing pathways of dipeptide-functionalized phosphine P6 catalyzed [3+2] annulation of acrylate with allenoates.

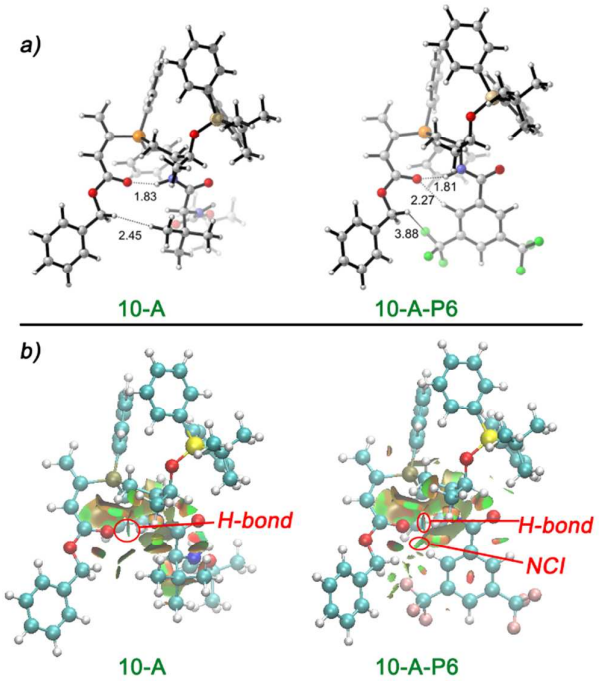

Figure 9. (a) Optimized structures of **10-A** and **10-A-P6**. (b) NCIPLOT of **10-A** and **10-A-P6**. The *s* = 0.6 au isosurface is colored according to a BGR scheme over the range $-0.05 < \mathrm{sign}(\lambda_2)\rho < 0.05$ au. Blue indicates strong attraction weak interaction, green indicates very weak interaction, and red indicates strong repulsion.

CONCLUSION

In summary, we studied the mechanism and the origins of enantioselectivities of phosphine-catalyzed [3+2] cycloadditions between allenoates and acrylate or imine. The combination of theoretical and experimental studies confirmed that appropriate hydrogen bond model and non-covalent interactions are crucial for observed enantioselectivities. For the acrylate substrates, the reaction preferentially proceeds via an intramolecular H-bond model. The hydrogen bond between allenoate and amide group of catalyst locks the configuration of zwitterionic catalyst-activated allenoate. The NCIPLOT analysis suggest that 2-naphthyl ester moiety exhibits stronger non-covalent interactions than the phenyl moiety, and such a significant substituent effect of acrylate substrate leads to the favorable *re*-face attack pathway. For imine substrate, the intermolecular H-bond model is more appropriate. In transition state **Ts3-I-*S1***, *n*-propyl group is oriented toward the pocket of catalyst, whereas in transition state **Ts2-I-*R1***, hydrogen atom arranged in the bulky pocket of the catalyst. Therefore, steric factors make the more crowded transition state **Ts3-I-*S1*** less stable than transition state **Ts2-I-*R1***.

All the theoretical studies carried out in this report agreed well with our experimental observations. More importantly, the insights gained in this study, the single hydrogen bond interacting model in particular, provide theoretical guidance for screening of catalysts and facilitate the design of more

effective catalytic systems. We are currently evolving more simplified amino acid-derived bifunctional phosphines based on the findings disclosed herein.

EXPERIMENTAL SECTION

General Information. Commercially available materials purchased from Alfa Aesar, Sigma-Aldrich, or TCI were used as received. Proton nuclear magnetic resonance (^{1}H NMR) spectra were recorded on a Bruker (400 MHz) spectrometer. Chemical shifts were recorded in parts per million (ppm, δ) relative to tetramethylsilane (δ 0.00) or chloroform (δ = 7.26, singlet). ^{1}H NMR splitting patterns are designated as s (singlet), d (doublet), t (triplet), q (quartet), dd (doublet of doublets); m (multiplets), and etc. All first-order splitting patterns were assigned on the basis of the appearance of the multiplet. Splitting patterns that could not be easily interpreted are designated as m (multiplet) or br (broad). Carbon nuclear magnetic resonance (^{13}C NMR) spectra were recorded on a Bruker (400 MHz) (100 MHz) spectrometer. The determination of *ee* was performed via chiral HPLC analysis using Shimadzu LC-20AD HPLC workstation. Visualization was performed using a UV lamp.

General procedures. Substrate **4** and **5**[17] and catalyst **P1**[16g] was synthesized according to the literature procedures.

To a 4 mL vial equipped with a magnetic stirring bar were added the phosphine catalyst **P1** (0.01 mmol) and acrylate **5** (0.1 mmol), followed by the addition of toluene (1 mL). Allenoate **4** (0.12 mmol) was then added, and the reaction mixture was stirred at room temperature for 1h. Then the mixture was subjected directly to flash column chromatographic separation using a mixture of hexane/ethyl acetate (10 : 1) as the eluent to afford cycloaddtion products **7-*S***.

Characterization of substrates and products.

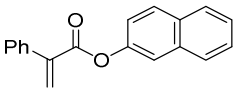

naphthalen-2-yl 2-phenylacrylate (5)

White solid. ^{1}H NMR (400 MHz, $CDCl_3$) δ 7.90-7.82 (m, 3H), 7.67 (d, *J* = 2.0 Hz, 1H), 7.58-7.56 (m, 2H), 7.53-7.46 (m, 2H), 7.45-7.37 (m, 3H), 7.33 (dd, *J* = 8.8, 2.2 Hz, 1H), 6.68 (d, *J* = 0.7 Hz, 1H), 6.13 (d, *J* = 0.7 Hz, 1H); ^{13}C NMR (100 MHz, $CDCl_3$) δ 165.4, 148.5, 140.9, 136.4, 133.8, 131.5, 129.4, 128.5, 128.4, 128.3, 127.8, 127.7, 126.6, 125.8, 121.1, 118.6; LCMS (ESI, m/z): calcd. for $C_{19}H_{15}O_2^+$ 275.1, found 275.1.

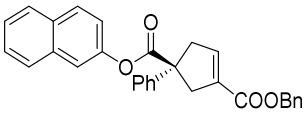

3-benzyl 1-(naphthalen-2-yl) (S)-1-phenylcyclopent-3-ene-1,3-dicarboxylate (7-*S*)

Colorless oil. ^{1}H NMR (400 MHz, $CDCl_3$) δ 7.82-7.74 (m, 3H), 7.51-7.32 (m, 13H), 7.03 (dd, *J* = 8.9, 2.3 Hz, 1H), 6.93 (m, 1H), 5.26 (s, 2H), 3.92 (dd, *J* = 16.5, 1.4 Hz, 1H), 3.83 (d, *J* = 17.6 Hz, 1H), 3.27 (dq, *J* = 16.5, 2.2 Hz, 1H), 3.09 (dq, *J* = 18.3, 2.2 Hz, 1H); ^{13}C NMR (100 MHz, $CDCl_3$) δ 174.0, 164.2, 148.6, 142.1, 141.6, 136.0, 134.7, 133.7, 131.5, 129.4, 128.9, 128.6, 128.3, 128.2, 127.8, 127.6, 127.5, 126.6, 125.7, 120.6, 118.2, 66.3, 58.6, 43.5, 41.4; LCMS (ESI, m/z): calcd. for $C_{30}H_{25}O_4^+$ 449.2, found 449.2; HPLC analysis (Chiralcel IB, Hexane/2-PrOH = 95/5, 1.00 mL/min), Rt = 10.6 min & 12.0 min.

ASSOCIATED CONTENT

Supporting Information. Cartesian coordinates and energies of all reported structures, full authorship of Gaussian 09 and NMR spectra. This material is available free of charge via the Internet at http://pubs.acs.org.

AUTHOR INFORMATION

Corresponding Author

*(R. Bai) E-mail: ruopeng@cqu.edu.cn

*(Y. Lu) E-mail: chmlyx@nus.edu.sg

*(Y. Lan) E-mail: lanyu@cqu.edu.cn

ORCID

Zhaoyuan Yu: 0000-0002-9570-3512

Ruopeng Bai: 0000-0002-1097-8526

Yixin Lu: 0000-0002-5730-166X

Yu Lan: 0000-0002-2328-0020

Notes

The authors declare no competing financial interest.

ACKNOWLEDGMENT

This work was supported by the National Natural Science Foundation of China (Grants 21372266 and 21772020). This work was supported by the China Scholarship Council.

REFERENCES

[1] (a) Rewcastle, G. W.; Baguley, B. C.; Cain, B. F. Potential Antitumor Agents. 37. Organophosphorus Derivatives of 9-Anilinoacridine. *J. Med. Chem*. **1982**, *25*, 1231–1235. (b) Serdar, C. M.; Gibson, D. T. Enzymatic Hydrolysis of Organophosphates: Cloning and Expression of A Parathion Hydrolase Gene from Pseudomonas Diminuta. *Bio/Technology* **1985**, *3*, 567–571. (c) Leca, D.; Fensterbank, L.; Lacôte, E.; Malacria, M. Recent Advances in the Use of Phosphorus-centered Radicals in Organic Chemistry. *Chem. Soc. Rev*. **2005**, *34*, 858–865. (d) Baumgartner, T.; Réau, R. Organophosphorus π-Conjugated Materials. *Chem. Rev*. **2006**, *106*, 4681–4727. (e) Gaunt, M. J.; Johansson, C. C. C.; McNally, A.; Vo, N. T. Enantioselective Organocatalysis. *Drug Discovery Today* **2007**, *12*, 8–27. (f) Pandey, V. K.; Dwivedi, A.; Pandey, O. P.; Sengupta, S. K. Organophosphorus Derivatives Containing Isatin-3-hydrazones as Chemotherapeutants against Fungal Pathogens of Sugarcane. *J. Agric. Food Chem*. **2008**, *56*, 10779–10784. (g) Grondal, C.; Jeanty, M.; Enders, D. Organocatalytic Cascade Reactions as a New Tool in Total Synthesis. *Nature Chem*. **2010**, *2*, 167–178. (h) Joly, D.; Bouit, P. A.; Hissler, M. Organophosphorus Derivatives for Electronic Devices. *J. Mater. Chem. C* **2016**, *4*, 3686–3698.

[2] (a) Noyori, R. BINAP: An Efficient Chiral Element for Asymmetric Catalysis. *Acc. Chem. Res*. **1990**, *23*, 345–350. (b) Hayashi, T. Chiral Monodentate Phosphine Ligand MOP for Transition-Metal-Catalyzed Asymmetric Reactions. *Acc. Chem. Res*. **2000**, *33*, 354–362. (c) Tang, W.; Zhang, X. New Chiral Phosphorus Ligands for Enantioselective Hydrogenation. *Chem. Rev*. **2003**, *103*, 3029–3069. (d) Tietze, L. F.; Ila, H.; Bell, H. P. Enantioselective Palladium-Catalyzed Transformations. *Chem. Rev*. **2004**, *104*, 3453–3516. (e) Xie, J.-H.; Zhou, Q.-L. Chiral Diphosphine and Monodentate Phosphorus Ligands on a Spiro Scaffold for Transition-Metal-Catalyzed Asymmetric Reactions. *Acc. Chem. Res*. **2008**, *41*, 581–593. (f) Teichert, J. F.; Feringa, B. L. Phosphoramidites: Privileged Ligands in Asymmetric Catalysis. *Angew. Chem., Int. Ed*. **2010**, *49*, 2486–2528.

[3] (a) Wolfe, J. P.; Wagaw, S.; Buchwald, S. L. An Improved Catalyst System for Aromatic Carbon–Nitrogen Bond Formation: The Possible Involvement of Bis(Phosphine) Palladium Complexes as Key Intermediates. *J. Am. Chem. Soc.* **1996**, *118*, 7215–7216. (b) Yanagisawa, A.; Matsumoto, Y.; Nakashima, H.; Asakawa, K.; Yamamoto, H. Enantioselective Aldol Reaction of Tin Enolates with Aldehydes Catalyzed by BINAP·Silver(I) Complex. *J. Am. Chem. Soc.* **1997**, *119*, 9319–9320. (c) Evans, D. A.; Thomson, R. J. Ni(II) Tol-BINAP-Catalyzed Enantioselective Orthoester Alkylations of N-Acylthiazolidinethiones. *J. Am. Chem. Soc.* **2005**, *127*, 10506–10507. (d) Wang, S.-Y.; Ji, S.-J.; Loh, T.-P. Cu(I) Tol-BINAP-Catalyzed Enantioselective Michael Reactions of Grignard Reagents and Unsaturated Esters. *J. Am. Chem. Soc.* **2007**, *129*, 276–277.

[4] (a) Lu, X.; Zhang, C.; Xu, Z. Reactions of Electron-Deficient Alkynes and Allenes under Phosphine Catalysis. *Acc. Chem. Res*. **2001**, *34*, 535–544. (b) Methot, J. L.; Roush, W. R. Nucleophilic Phosphine Organocatalysis. *Adv. Synth. Catal*. **2004**, *346*, 1035–1050. (c) Ye, L.-W.; Zhou, J.; Tang, Y. Phosphine-Triggered Synthesis of Functionalized Cyclic Compounds. *Chem. Soc. Rev*. **2008**, *37*, 1140–1152. (d) Cowen, B. J.; Miller, S. J. Enantioselective Catalysis and Complexity Generation from Allenoates. *Chem. Soc. Rev*. **2009**, *38*, 3102–3116. (e) Marinetti, A.; Voituriez, A. Enantioselective Phosphine Organocatalysis. *Synlett* **2010**, 174–194. (f) Wang, T.; Han, X.; Zhong, F.; Yao, W.; Lu, Y. Amino Acid-Derived Bifunctional Phosphines for Enantioselective Transformations. *Acc. Chem. Res*. **2016**, *49*, 1369–1378.

[5] (a) Aroyan, C. E.; Dermenci, A.; Miller, S. J. The Rauhut–Currier Reaction: A History and its Synthetic

Application. *Tetrahedron* **2009**, *65*, 4069–4084. (b) Takizawa, S.; Nguyen, T. M.-N.; Grossmann, A.; Enders, D.; Sasai, H. Enantioselective Synthesis of α-Alkylidene-γ-Butyrolactones: Intramolecular Rauhut–Currier Reaction Promoted by Acid/Base Organocatalysts. *Angew. Chem., Int. Ed*. **2012**, *51*, 5423–5426. (c) Shi, Z.; Tong, Q.; Leong, W. W. Y.; Zhong, G. [4+2] Annulation of Vinyl Ketones Initiated by a Phosphine-Catalyzed Aza-Rauhut–Currier Reaction: A Practical Access to Densely Functionalized Tetrahydropyridines. *Chem.—Eur. J*. **2012**, *18*, 9802–9806. (d) Su, X.; Zhou, W.; Li, Y.; Zhang, J. Design, Synthesis, and Application of a Chiral Sulfinamide Phosphine Catalyst for the Enantioselective Intramolecular Rauhut–Currier Reaction. *Angew. Chem., Int. Ed*. **2015**, *54*, 6874–6877.

[6] (a) Cho, C.-W.; Kong, J.-R.; Krische, M. J. Phosphine-Catalyzed Regiospecific Allylic Amination and Dynamic Kinetic Resolution of Morita−Baylis−Hillman Acetates. *Org. Lett*. **2004**, *6*, 1337–1339. (b) Masson, G.; Housseman, C.; Zhu, J. The Enantioselective Morita–Baylis–Hillman Reaction and Its Aza Counterpart. *Angew. Chem., Int. Ed*. **2007**, *46*, 4614–4628. (c) Takizawa, S.; Inoue, N.; Hirata, S.; Sasai, H. Enantioselective Synthesis of Isoindolines: An Organocatalyzed Domino Process Based On the aza-Morita–Baylis–Hillman Reaction. *Angew. Chem., Int. Ed*. **2010**, *49*, 9725–9729. (d) Takizawa, S.; Kiriyama, K.; Ieki, K.; Sasai, H. A Bifunctional Spiro-type Organocatalyst With High Enantiocontrol: Application to the aza-Morita–Baylis–Hillman Reactions. *Chem. Commun*. **2011**, *47*, 9227–9229. (e) Hu, F.-L.; Wei, Y.; Shi, M. Phosphine-Catalyzed Asymmetric [4+1] Annulation of Activated α,β-unsaturated Ketones with Morita–Baylis–Hillman Carbonates: Enantioselective Synthesis of Spirooxindoles Containing Two Adjacent Quaternary Stereocenters. *Chem. Commun*. **2014**, *50*, 8912–8914.

[7] (a) Sriramurthy, V.; Barcan, G. A.; Kwon, O. Bisphosphine-Catalyzed Mixed Double-Michael Reactions: Asymmetric Synthesis of Oxazolidines, Thiazolidines, and Pyrrolidines. *J. Am. Chem. Soc*. **2007**, *129*, 12928–12929. (b) Li, G.-Z.; Randev, R. K.; Soeriyadi, A. H.; Rees, G.; Boyer, C.; Tong, Z.; Davis, T. P.; Becer, C. R.; Haddleton, D. M. Investigation into Thiol-(meth)acrylate Michael Addition Reactions using Amine and Phosphine Catalysts. *Polym. Chem*. **2010**, *1*, 1196–1204. (c) Baslé, O.; Porcel, S.; Ladeira, S.; Bouhadir, G.; Bourissou, D. Phosphine-boronates: Efficient Bifunctional Organocatalysts for Michael Addition. *Chem. Commun*. **2012**, *48*, 4495–4497.

[8] (a) Vedejs, E.; Diver, S. T. Tributylphosphine: A Remarkable Acylation Catalyst. *J. Am. Chem. Soc.* **1993**, *115*, 3358–3359. (b) Trost, B. M.; Li, C.-J. Novel "Umpolung" in C–C Bond Formation Catalyzed by Triphenylphosphine. *J. Am. Chem. Soc.* **1994**, *116*, 3167–3168. (c) Na, R.; Jing, C.; Xu, Q.; Jiang, H.; Wu, X.; Shi, J.; Zhong, J.; Wang, M.; Benitez, D.; Tkatchouk, E.; Goddard, W. A.; Guo, H.; Kwon, O. Phosphine-Catalyzed Annulations of Azomethine Imines: Allene-Dependent [3+2], [3+3], [4+3], and [3+2+3] Pathways. *J. Am. Chem. Soc*. **2011**, *133*, 13337–13348. (d) Yu, P.; Zheng, S.-C.; Yang, N.-Y.; Tan, B.; Liu, X.-Y. Phosphine-Catalyzed Remote β-C–H Functionalization of Amines Triggered by Trifluoromethylation of Alkenes: One-Pot Synthesis of Bistrifluoromethylated Enamides and Oxazoles. *Angew. Chem., Int. Ed*. **2015**, *54*, 4041–4045. (e) Zhang, J.; Lin, S.-X.; Cheng, D.-J.; Liu, X.-Y.; Tan, B. Phosphoric Acid-Catalyzed Asymmetric Classic Passerini Reaction. *J. Am. Chem. Soc*. **2015**, *137*, 14039–14042.

[9] Zhang, C.; Lu, X. Phosphine-Catalyzed Cycloaddition of 2,3-Butadienoates or 2-Butynoates with Electron-Deficient Olefins. A novel [3+ 2] Annulation Approach to Cyclopentenes. *J. Org. Chem*. **1995**, *60*, 2906–2908.

[10] Zhu, G.; Chen, Z.; Jiang, Q.; Xiao, D.; Cao, P.; Zhang, X. Asymmetric [3+2] Cycloaddition of 2,3-Butadienoates with Electron-Deficient Olefins Catalyzed by Novel Chiral 2,5-Dialkyl-7-phenyl-7-phosphabicyclo[2.2.1]heptanes. *J. Am. Chem. Soc.* **1997**, *119*, 3836–3837.

[11] Wilson, J. E.; Fu, G. C. Synthesis of Functionalized Cyclopentenes through Catalytic Asymmetric [3+2] Cycloadditions of Allenes with Enones. *Angew. Chem., Int. Ed*. **2006**, *45*, 1426–1429.

[12] Cowen, B. J. Miller, S. J. Enantioselective [3+2]-Cycloadditions Catalyzed by a Protected, Multifunctional Phosphine-Containing α-Amino Acid. *J. Am. Chem. Soc.* **2007**, *129*, 10988–10989.

[13] (a) Xiao, H.; Chai, Z.; Zheng, C.-W.; Yang, Y.-Q.; Liu, W.; Zhang, J.-K.; Zhao, G. Asymmetric [3+2] Cycloadditions of Allenoates and Dual Activated Olefins Catalyzed by Simple Bifunctional N-Acyl Aminophosphines. *Angew. Chem., Int. Ed*. **2010**, *49*, 4467–4470. (b) Sampath, M.; Loh, T.-P. Highly Enantio-, Regio- and Diastereo-Selective one-pot [2+3]-Cycloaddition Reaction via Isomerization of 3-Butynoates to Allenoates. *Chem. Sci*. **2010**, *1*, 739–742. (c) Zhong, F.; Chen, G.-Y.; Han, X.; Yao, W.; Lu, Y. Asymmetric Construction of Functionalized Bicyclic Imides via [3+2] Annulation of MBH Carbonates Catalyzed by Dipeptide-Based Phosphines. *Org. Lett*. **2012**, *14*, 3764–3767. (d) Zhang, X.-N.; Shi, M. Phosphine-Catalyzed [3+2] Cycloaddition of 4,4-Dicyano-2-methylenebut-3-enoates with Benzyl Buta-2,3-dienoate and Penta-3,4-dien-2-one. *ACS Catal*. **2013**, *3*, 507–512. (e) Gicquel, M.; Zhang, Y.; Aillard, P.; Retailleau, P.; Voituriez, A.; Marinetti, A. Phosphahelicenes in Asymmetric Organocatalysis: [3+2] Cyclizations of γ-Substituted Allenes and Electron-Poor Olefins. *Angew. Chem., Int. Ed*. **2015**, *54*, 5470–5473. (f) Lee, S. Y.; Fujiwara, Y.; Nishiguchi, A.; Kalek, M.; Fu, G. C. Phosphine-Catalyzed Enantioselective Intramolecular [3+2] Annulations To Generate Fused Ring Systems. *J. Am. Chem. Soc.* **2015**, *137*, 4587–4591.

[14] (a) Pellissier, H. Asymmetric Domino Reactions. Part B: Reactions Based on the Use of Chiral Catalysts and Biocatalysts. *Tetrahedron* **2006**, *62*, 2143–2173. (b) Bolm, C.; Rantanen, T.; Schiffers, I.; Zani, L. Protonated Chiral Catalysts: Versatile Tools for Asymmetric Synthesis. *Angew. Chem., Int. Ed*. **2005**, *44*, 1758–1763. (c) Deng, H.-P.; Wei, Y.; Shi, M. Highly Regio- and Diastereoselective Construction of Spirocyclopenteneoxindoles through Phosphine-Catalyzed [3+2] Annulation of Morita–Baylis–Hillman Carbonates with Isatylidene Malononitriles. *Org. Lett*. **2011**, *13*, 3348–3351. (d) Tan, B.; Candeias, N. R.; Barbas, C. F., III Core-Structure-Motivated Design of a Phosphine-Catalyzed [3+2] Cycloaddition Reaction: Enantioselective Syntheses of Spirocyclopenteneoxindoles. *J. Am. Chem. Soc.* **2011**, *133*, 4672–4675. (e) Fujiwara, Y.; Fu, G. C. Application of a New Chiral Phosphepine to the Catalytic Asymmetric Synthesis of Highly Functionalized Cyclopentenes That Bear an Array of Heteroatom-Substituted Quaternary Stereocenters. *J. Am. Chem. Soc.* **2011**, *133*, 12293–12297.

[15] (a) Jarvo, E. R.; Miller, S. J. Amino Acids and Peptides as Asymmetric Organocatalysts. *Tetrahedron* **2002**, *58*, 2481–2495. (b) List, B. Proline-Catalyzed Asymmetric Reactions. *Tetrahedron* **2002**, *58*, 5573–5590. (c) Notz, W.; Tanaka, F.; Barbas, C. F., III Enamine-Based Organocatalysis with Proline and Diamines: The Development of Direct Catalytic Asymmetric Aldol, Mannich, Michael, and Diels-Alder Reactions. *Acc. Chem. Res*. **2004**, *37*, 580–591. (d) Xu, L.-W.; Lu, Y. Primary Amino Acids: Privileged Catalysts in Enantioselective Organocatalysis. *Org. Biomol. Chem*. **2008**, *6*, 2047–2053. (e) MacMillan, D. W. C. The Advent and Development of Organocatalysis. *Nature* **2008**, *455*, 304–308. (f) Mohr, J. T.; Krout, M. R.; Stoltz, B. M. Natural Products as Inspiration for the Development of Asymmetric Catalysis. *Nature* **2008**, *455*, 323–332. (g) Wennemers, H. Asymmetric catalysis with

Peptides. *Chem. Commun*. **2011**, *47*, 12036–12041.

[16] (a) Notz, W.; List, B. Catalytic Asymmetric Synthesis of *anti*-1,2-Diols. *J. Am. Chem. Soc.* **2000**, *122*, 7386–7387. (b) List, B.; Pojarliev, P.; Biller, W. T.; Martin, H. J. The Proline-Catalyzed Direct Asymmetric Three-Component Mannich Reaction: Scope, Optimization, and Application to the Highly Enantioselective Synthesis of 1,2-Amino Alcohols. *J. Am. Chem. Soc.* **2002**, *124*, 827–833. (c) Kumaragurubaran, N.; Juhl, K.; Zhuang, W.; Bøgevig, A.; Jørgensen, K. A. Direct L-Proline-Catalyzed Asymmetric α-Amination of Ketones. *J. Am. Chem. Soc.* **2002**, *124*, 6254–6255. (d) Imbriglio, J. E.; Vasbinder, M. M.; Miller, S. J. Dual Catalyst Control in the Amino Acid-Peptide-Catalyzed Enantioselective Baylis−Hillman Reaction. *Org. Lett*. **2003**, *5*, 3741–3743. (e) Wang, W.; Wang, J.; Li, H. Direct, Highly Enantioselective Pyrrolidine Sulfonamide Catalyzed Michael Addition of Aldehydes to Nitrostyrenes. *Angew. Chem., Int. Ed*. **2005**, *44*, 1369–1371. (f) Zhou, L.; Tan, C. K.; Jiang, X.; Chen, F.; Yeung, Y.-Y. Asymmetric Bromolactonization Using Amino-thiocarbamate Catalyst. *J. Am. Chem. Soc.* **2010**, *132*, 15474–15476. (g) Zhong, F.; Han, X.; Wang, Y.; Lu, Y. Highly enantioselective [4 + 2] annulations catalyzed by amino acid-based phosphines: Synthesis of functionalized cyclohexenes and 3-spirocyclohexene-2-oxindoles. *Chem. Sci.* **2012**, *3*, 1231–1234. (h) Ni, H.; Tang, X.; Zheng, W.; Yao, W.; Ullah, N.; Lu, Y. Enantioselective Phosphine-Catalyzed Formal [4+4] Annulation of α,β-Unsaturated Imines and Allene Ketones: Construction of Eight-Membered Rings. *Angew. Chem., Int. Ed*. **2017**, *56*, 14222–14226.

[17] Han, X.; Wang, Y.; Zhong, F.; Lu, Y. Enantioselective [3+2] Cycloaddition of Allenes to Acrylates Catalyzed by Dipeptide-Derived Phosphines: Facile Creation of Functionalized Cyclopentenes Containing Quaternary Stereogenic Centers. *J. Am. Chem. Soc.* **2011**, *133*, 1726–1729.

[18] Han, X.; Zhong, F.; Wang, Y.; Lu, Y. Versatile Enantioselective [3+2] Cyclization between Imines and Allenoates Catalyzed by Dipeptide-Based Phosphines. *Angew. Chem., Int. Ed*. **2012**, *51*, 767–770.

[19] (a) Allemann, C.; Gordillo, R.; Clemente, F. R.; Cheong, P.- Y.; Houk, K. N. Theory of Asymmetric Organocatalysis of Aldol and Related Reactions: Rationalizations and Predictions. *Acc. Chem. Res*. **2004**, *37*, 558–569. (b) Taylor, M. S.; Jacobsen, E. N. Asymmetric Catalysis by Chiral Hydrogen-Bond Donors. *Angew. Chem., Int. Ed*. **2006**, *45*, 1520–1543. (c) Yu, X.; Wang, W. Hydrogen-Bond-Mediated Asymmetric Catalysis. *Chem.—Asian J.* **2008**, *3*, 516–532. (d) Lam, Y.-H.; Grayson, M. N.; Holland, M. C.; Simon, A.; Houk, K. N. Theory and Modeling of Asymmetric Catalytic Reactions. *Acc. Chem. Res*. **2016**, *49*, 750–762. (e) Wheeler, S. E.; Seguin, T. J.; Guan, Y.; Doney, A. C. Noncovalent Interactions in Organocatalysis and the Prospect of Computational Catalyst Design. *Acc. Chem. Res*. **2016**, *49*, 1061–1069. (f) Reid, J. P.; Simón, L.; Goodman, J. M. A Practical Guide for Predicting the Stereochemistry of Bifunctional Phosphoric Acid Catalyzed Reactions of Imines. *Acc. Chem. Res*. **2016**, *49*, 1029–1041. (g) Cui, C.-X.; Shan, C.; Zhang, Y.-P.; Chen, X.-L.; Qu, L.-B.; Lan, Y. Mechanism of Phosphine-Catalyzed Allene Coupling Reactions: Advances in Theoretical Investigations. *Chem.—Asian J*. **2018**, *13*, 1076–1088.

[20] Frisch, M. J.; et al. *Gaussian 09*; Revision D.01; Gaussian, Inc.: Wallingford, CT, 2013.

[21] (a) Becke, A. D. Density-Functional Thermochemistry. III. The Role of Exact Exchange. *J. Chem. Phys*. **1993**, *98*, 5648–5652. (b) Lee, C.; Yang, W.; Parr, R. G. Development of the Colle-Salvetti Correlation-Energy Formula into a Functional of the Electron Density. *Phys. Rev. B: Condens. Matter Mater. Phys*. **1988**, *37*, 785–789. (c) Stephens, P. J.; Devlin, F. J. Chabalowski, C. F.; Frisch, M. J. *Ab Initio* Calculation of Vibrational Absorption and Circular Dichroism Spectra Using Density Functional Force Fields. *J. Phys. Chem*. **1994**, *98*, 11623–11627.

[22] (a) Hehre, W. J.; Ditchfield, R.; Pople, J. A. Self—Consistent Molecular Orbital Methods. XII. Further Extensions of Gaussian—Type Basis Sets for Use in Molecular Orbital Studies of Organic Molecules. *J. Chem. Phys*. **1972**, *56*, 2257–2261. (b) Dill, J. D.; Pople, J. A. Selfconsistent Molecular Orbital Methods. XV. Extended Gaussiantype Basis Sets for Lithium, Beryllium, and Boron. *J. Chem. Phys*. **1975**, *62*, 2921–2923. (c) Francl, M. M.; Pietro, W. J.; Hehre, W. J.; Binkley, J. S.; Gordon, M. S.; DeFrees, D. J.; Pople, J. A. Selfconsistent Molecular Orbital Methods. XXIII. A Polarizationtype Basis Set for Second Row Elements. *J. Chem. Phys*. **1982**, *77*, 3654–3665.

[23] (a) Yao, W.; Yu, Z.; Wen, S.; Ni, H.; Ullah, N.; Lan, Y.; Lu, Y. Chiral Phosphine-mediated Intramolecular [3+2] Annulation: Enhanced Enantioselectivity by Achiral Brønsted Acid. *Chem. Sci*. **2017**, *8*, 5196–5200. (b) Ni, H.; Yu, Z.; Yao, W.; Lan, Y.; Ullah, N.; Lu, Y. Catalyst-Controlled Regioselectivity in Phosphine Catalysis: The Synthesis of Spirocyclic Benzofuranones via Regiodivergent [3+2] Annulations of Aurones and an Allenoate. *Chem. Sci*. **2017**, *8*, 5699–5704. (c) Yu, Z.; Lan, Y. Mechanism of Rhodium-Catalyzed Carbon–Silicon Bond Cleavage for the Synthesis of Benzosilole Derivatives: A Computational Study. *J. Org. Chem*. **2013**, *78*, 11501–11507. (d) Duan, M.; Zhu, L.; Qi, X.; Yu, Z.; Li, Y.; Bai, R.; Lan, Y. From Mechanistic Study to Chiral Catalyst Optimization: Theoretical Insight into Binaphthophosphepine-catalyzed Asymmetric Intramolecular [3+2] Cycloaddition. *Sci. Rep*. **2017**, *7*, 7619–7631.

[24] Peverati, R.; Truhlar, D. G. Improving the Accuracy of Hybrid Meta-GGA Density Functionals by Range Separation. *J. Phys. Chem. Lett*. **2011**, *2*, 2810–2817.

[25] (a) Krishnan, R.; Binkley, J. S.; Seeger, R.; Pople, J. A. Self-Consistent Molecular Orbital Methods. XX. A Basis Set for Correlated Wave Functions. *J. Chem. Phys*. **1980**, *72*, 650–654. (b) McLean, A. D.; Chandler, G. S. Contracted Gaussian Basis Sets for Molecular Calculations. I. Second Row Atoms, Z=11–18. *J. Chem. Phys*. **1980**, *72*, 5639–5648.

[26] (a) Cancès, E.; Mennucci, B.; Tomasi, J. A New Integral Equation Formalism for the Polarizable Continuum Model: Theoretical Background and Applications to Isotropic and Anisotropic Dielectrics. *J. Chem. Phys*. **1997**, *107*, 3032–3041. (b) Cancès, E.; Mennucci, B. New Applications of Integral Equations Methods for Solvation Continuum Models: Ionic Solutions and Liquid Crystals. *J. Math. Chem*. **1998**, *23*, 309–326. (c) Mennucci, B.; Cancès, E.; Tomasi, J. Evaluation of Solvent Effects in Isotropic and Anisotropic Dielectrics and in Ionic Solutions with a Unified Integral Equation Method: Theoretical Bases, Computational Implementation, and Numerical Applications. *J. Phys. Chem. B*, **1997**, *101*, 10506–10517. (d) Scalmani, G.; Frisch, M. J. Continuous Surface Charge Polarizable Continuum Models of Solvation. I. General Formalism. *J. Chem. Phys*. **2010**, *132*, 114110–114124.

[27] Lu, T.; Chen, F. Multiwfn: A Multifunctional Wavefunction Analyzer. *J. Comput. Chem*. **2012**, *33*, 580–592.

[28] Humphrey, W.; Dalke, A.; Schulten, K. VMD: Visual Molecular Dynamics. *J. Molec. Graphics*. **1996**, *44*, 33–38.

[29] Legault, C. Y. CYL*view, 1.0b*; Université de Sherbrooke, 2009 (http://www.cylview.org).

[30] (a) Xia, Y.; Liang, Y.; Chen, Y.; Wang, M.; Jiao, L.; Huang, F.; Liu, S.; Li, Y.; Yu, Z.-X. An Unexpected Role of a Trace Amount of Water in Catalyzing Proton Transfer in Phosphine-Catalyzed (3+2) Cycloaddition of Allenoates

and Alkenes. *J. Am. Chem. Soc.* **2007**, *129*, 3470–3471. (b) Mercier, E.; Fonovic, B.; Henry, C.; Kwon, O.; Dudding, T. Phosphine Triggered [3+2] Allenoate–Acrylate Annulation: A Mechanistic Enlightenment. *Tetrahedron Lett*. **2007**, *48*, 3617–3620. (c) Zhao, L.; Wen, M.; Wang, Z.-X. Reaction Mechanism of Phosphane-Catalyzed [4+2] Annulations between α-Alkylallenoates and Activated Alkenes: A Computational Study. *Eur. J. Org. Chem*. **2012**, 3587–3597. (d) Qiao, Y.; Han, K.-L. Elucidation of the Reaction Mechanisms and Diastereoselectivities of Phosphine-Catalyzed [4+2] Annulations between Allenoates and Ketones or Aldimines. *Org. Biomol. Chem*. **2012**, *10*, 7689–7706. (e) Huang, G.-T.; Lankau, T.; Yu, C.-H. A Computational Study: Reactivity Difference between Phosphine-and Amine-Catalyzed Cycloadditions of Allenoates and Enones. *J. Org. Chem.* **2014**, *79*, 1700–1711.

[31] (a) Knowles, R. R.; Jacobsen, E. N. Attractive Noncovalent Interactions in Asymmetric Catalysis: Links between Enzymes and Small Molecule Catalysts. *Proc. Natl. Acad. Sci. U. S. A*. **2010**, *107*, 20678–20685. (b) Uyeda, C.; Jacobsen, E. N. Transition-State Charge Stabilization through Multiple Non-covalent Interactions in the Guanidinium-Catalyzed Enantioselective Claisen Rearrangement. *J. Am. Chem. Soc.* **2011**, *133*, 5062–5075. (c) Lin, S.; Jacobsen, E. N. Thiourea-Catalysed Ring Opening of Episulfonium Ions with Indole Derivatives by Means of Stabilizing Non-Covalent Interactions. *Nature Chem*. **2012**, *4*, 817–824. (d) Brown, A. R.; Uyeda, C.; Brotherton, C. A. Jacobsen, E. N. Enantioselective Thiourea-Catalyzed Intramolecular Cope-Type Hydroamination. *J. Am. Chem. Soc.* **2013**, *135*, 6747–6749.

[32] (a) Jiang, H.; Paixão, M. W.; Monge, D.; Jørgensen, K. A. Acyl Phosphonates: Good Hydrogen Bond Acceptors and Ester/Amide Equivalents in Asymmetric Organocatalysis. *J. Am. Chem. Soc.* **2010**, *132*, 2775–2783. (b) Albrecht, L.; Dickmeiss, G.; Acosta, F. C.; Rodríguez-Escrich, C.; Davis, R. L.; Jørgensen, K. A. Asymmetric Organocatalytic Formal [2+2]-Cycloadditions via Bifunctional H-Bond Directing Dienamine Catalysis. *J. Am. Chem. Soc.* **2012**, *134*, 2543–2546.

[33] (a) Simón, L.; Goodman, J. M. Mechanism of Amination of β-Keto Esters by Azadicarboxylates Catalyzed by an Axially Chiral Guanidine: Acyclic Keto Esters React through an *E* Enolate. *J. Am. Chem. Soc.* **2012**, *134*, 16869–16876. (b) Overvoorde, L. M.; Grayson, M. N.; Luo, Y.; Goodman, J. M. Mechanistic Insights into a BINOL-Derived Phosphoric Acid-Catalyzed Asymmetric Pictet−Spengler Reaction. *J. Org. Chem.* **2015**, *80*, 2634–2640.

[34] (a) Holland, M. C. Gilmour, R.; Houk, K. N. Importance of Intermolecular Hydrogen Bonding for the Stereo-chemical Control of Allene–Enone (3+2) Annulations Catalyzedby a Bifunctional, Amino Acid Derived Phosphine Catalyst. *Angew. Chem., Int. Ed*. **2016**, *55*, 2022–2027. (b) Bickelhaupt, F. M.; Houk, K. N. Analyzing Reaction Rates with the Distortion/Interaction-Activation Strain Model. *Angew. Chem., Int. Ed*. **2017**, *56*, 10070–10086.

[35] (a) Hamza, A.; Schubert, G.; Soós, T.; Pápai, I. Theoretical Studies on the Bifunctionality of Chiral Thiourea-Based Organocatalysts: Competing Routes to C−C Bond Formation. *J. Am. Chem. Soc.* **2006**, *128*, 13151–13160. (b) Duarte, F. J. S.; Santos, A. G. Enantioselective Organocatalytic Intramolecular Diels−Alder Reactions: A Computational Study. *J. Org. Chem.* **2012**, *77*, 3252–3261. (c) Aasheim, J. H.; Fliegl, H.; Uggerud, E.; Bonge-Hansen, T.; Eisenstein, O. Stereoselectivity through a Network of Non-Classical CH Weak Interactions: A Prospective Study of a Bicyclic Organocatalytic Scaffold. *New J. Chem*. **2014**, *38*, 5975–5982. (d) Armstrong, A.;

Boto, R. A.; Dingwall, P.; Contreras-García, J.; Harvey, M. J.; Mason, N. J.; Rzepa, H. S. The Houk–List Transition States for Organocatalytic Mechanisms Revisited. *Chem. Sci*. **2014**, *5*, 2057–2071. (e) Simón, L.; Paton, R. S. Origins of Asymmetric Phosphazene Organocatalysis: Computations Reveal a Common Mechanism for Nitro- and Phospho-Aldol Additions. *J. Org. Chem*. **2015**, *80*, 2756–2766. (f) Xue, Y.; Wang, Y.; Cao, Z.; Zhou, J.; Chen, Z.-X. Computational Insight into the Cooperative Role of Non-Covalent Interactions in the aza-Henry Reaction Catalyzed by Quinine Derivatives: Mechanism and Enantioselectivity. *Org. Biomol. Chem*. **2016**, *14*, 9588–9597.

[36] (a) Bassan, A.; Zou, W.; Reyes, E.; Himo, F.; Córdova, A. The Origin of Stereoselectivity in Primary Amino Acid Catalyzed Intermolecular Aldol Reactions. *Angew. Chem., Int. Ed*. **2005**, *44*, 7028–7032. (b) Moran, A.; Hamilton, A.; Bo, C.; Melchiorre, P. A Mechanistic Rationale for the 9-Amino(9-deoxy)*epi* Cinchona Alkaloids Catalyzed Asymmetric Reactions via Iminium Ion Activation of Enones. *J. Am. Chem. Soc*. **2013**, *135*, 9091–9098. (c) Kumari, P.; Barik, S.; Khan, N. H.; Ganguly, B.; Kureshy, R. I.; Abdi, S. H. R.; Bajaj, H. C. The Origin for Highly Enantioselective Induction of 1-Naphthol to Isatin-Derived *N*-Boc Ketimines Catalyzed by Quinine Thiourea Catalyst: An Experimental and Computational Study. *RSC Adv*. **2015**, *5*, 69493–69501. (d) Cheng, G.-J.; Zhang, X.; Chung, L. W.; Xu, L.; Wu, Y.-D. Computational Organic Chemistry: Bridging Theory and Experiment in Establishing the Mechanisms of Chemical Reactions. *J. Am. Chem. Soc*. **2015**, *137*, 1706–1725. (e) Monaco, M. R.; Fazzi, D.; Tsuji, N.; Leutzsch, M.; Liao, S.; Thiel, W.; List, B. The Activation of Carboxylic Acids via Self-Assembly Asymmetric Organocatalysis: A Combined Experimental and Computational Investigation. *J. Am. Chem. Soc*. **2016**, *138*, 14740–14749.

[37] Fang, Y.-Q.; Jacobsen, E. N. Cooperative, Highly Enantioselective Phosphinothiourea Catalysis of Imine–Allene [3+2] Cycloadditions. *J. Am. Chem. Soc*. **2008**, *130*, 5660–5661.

[38] (a) Wang, T.; Yu, Z.; Hoon, D. L.; Huang, K.-W.; Lan, Y.; Lu, Y. Highly Enantioselective Construction of Tertiary Thioethers and Alcohols via Phosphine-Catalyzed Asymmetric γ-Addition Reactions of 5*H*-Thiazol-4-Ones and 5*H*-Oxazol-4-Ones: Scope and Mechanistic Understandings. *Chem. Sci*. **2015**, *6*, 4912–4922. (b) Wang, T.; Yu, Z.; Hoon, D. L.; Phee, C. Y.; Lan, Y.; Lu, Y. Regiodivergent Enantioselective γ-Additions of Oxazolones to 2,3-Butadienoates Catalyzed by Phosphines: Synthesis of α,α-Disubstituted α-Amino Acids and *N,O*-Acetal Derivatives. *J. Am. Chem. Soc*. **2016**, *138*, 265–271.

[39] Johnson, E. R.; Keinan, S.; Mori-Sánchez, P.; Contreras-García, J.; Cohen, A. J.; Yang, W. Revealing Noncovalent Interactions. *J. Am. Chem. Soc*. **2010**, *132*, 6498–6506.